

films, which were prepared on quartz plates by spin coating from concentrated cluster solutions, are similar to the spectrum of an aqueous solution. The position of the maximum is, however, shifted to the red by approximately 5 nm. The luminescence spectrum of the crystalline solid is also similar to the solution spectrum (Fig. 5B) and is also shifted slightly to the red (~12 nm). Thus, small optical changes that might reflect cluster-cluster interactions in the solid samples could be observed.

In (7) we described the synthesis and characterization of differently sized 1-thioglycerol-stabilized CdS clusters. One of the prepared species displayed exactly the same optical behavior as 4. At that time, we speculated, on the basis of elemental analysis, small-angle x-ray scattering, and UV-VIS spectroscopy, that this sample might consist of Cd₁₇ clusters. However, attempts to crystallize this compound, which is readily water-soluble, have not been successful. Nevertheless, it should be possible to crystallize clusters of the type Cd₁₇S₄(RS)₂₆ with various thiolate ligands RS. This should lead to a set of different superlattices consisting of almost identical CdS cluster cores, which can be regarded as ideal systems for the study of collective phenomena based on cluster-cluster interactions.

REFERENCES AND NOTES

1. A. Henglein, *Top. Curr. Chem.* **143**, 113 (1988).
2. ———, *Chem. Rev.* **89**, 1861 (1989).
3. L. E. Brus, *Appl. Phys. A* **53**, 465 (1991).
4. Y. Wang and N. Herron, *J. Phys. Chem.* **95**, 525 (1991).
5. H. Weller, *Angew. Chem. Int. Ed. Engl.* **32**, 41 (1993).
6. ———, *Adv. Mater.* **5**, 88 (1993).
7. T. Vossmeier et al., *J. Phys. Chem.* **98**, 7665 (1994).
8. L. E. Brus, *ibid.* **80**, 4403 (1984).
9. N. Herron, J. C. Calabrese, W. E. Farneth, Y. Wang, *Science* **259**, 1426 (1993).
10. G. S. H. Lee et al., *J. Am. Chem. Soc.* **110**, 4863 (1988).
11. P. Strickler, *J. Chem. Soc. Chem. Commun.* **1969**, 655 (1969).
12. Diffraction data for the x-ray structure analysis were collected on an Enraf-Nonius (Delft, Netherlands) CAD4 diffractometer (graphite monochromatized MoK α radiation, wavelength of 0.7107 Å). The monoclinic cell parameters were determined from the Bragg angles of 25 computer-centered reflections as $a = 25.147(4)$ Å, $b = 40.096(5)$ Å, $c = 25.358(5)$ Å, and $\beta = 94.0(1)^\circ$ (error in the last digit in parentheses). The space group was assigned as $I2/a$ (no. 15), and the structure confirmed this assignment. The colorless, irregularly shaped crystals were very unstable, as indicated by the drastic loss in intensities during x-ray exposure. Therefore, three crystals (100 to 180 μm) sealed in capillaries were used for the data collection. Because of the instability and the weak diffraction power of the nonperfect crystals, only 5414 unique reflections with $I \geq 2\sigma(I)$ (where I is intensity) were measured in the range of $1.5^\circ \leq 2\theta \leq 38^\circ$ (θ is the dispersion angle). We solved the structure by direct methods and refined it by blocked full-matrix least squares techniques by using weighted restraints for the bond lengths and angles of the organic residues. Despite the poor quality of the available reflections, all C and O atoms could be located by difference Fourier synthesis. The final refinement of 587 parameters (data-to-parameter ratio = 9.2) in which only Cd was anisotropic converged at $R = 0.115$ (unit weights). This relatively high value may be attributable to the instability of the crystals, probably small structural changes during x-ray exposure, and rotational disorder of most of the organic residues indicated by the extreme high thermal parameters of some C and all O atoms. Additional data on this material can be ordered by referring to no. CSD-401359, names of the authors, and citation of the paper at the Fachinformationszentrum Karlsruhe, Gesellschaft für wissenschaftlich-technische Information mbH, D-76344 Eggenstein-Leopoldshafen, Germany.
13. Analysis calculated for C₅₂H₁₃₀O₂₆S₃₀Cd₁₇: C, 15.44%; H, 3.25%; O, 10.28%; S, 23.79%; and Cd, 47.24%. Found: C, 15.50%; H, 3.32%; O, 10.8%; S, 23.2%; and Cd, 46.5%.
14. R. A. Haberkorn et al., *Inorg. Chem.* **15**, 2408 (1976).
15. The observed signals of the ¹¹³Cd NMR spectrum, which are due to Cd atoms of the cluster surfaces and vertices (440 and 630 ppm) are most probably

broadened by exchange phenomena involving coordination by solvent molecules and OH groups of the organic residues. The involvement of OH groups is also indicated by ¹H NMR measurements; three temperature-dependent signals of hydroxyl protons were detected in DMF solution. The fact that the signal at 440 ppm could not be detected in DMF solution also indicates extensive exchange processes. However, because of the decreasing solubility of 4 in DMF with decreasing temperature, and decomposition at higher temperatures, no information could be obtained by temperature-dependent ¹¹³Cd NMR measurements.

16. A. D. Cardin, P. D. Ellis, J. D. Odom, J. W. Howard, *J. Am. Chem. Soc.* **97**, 1672 (1975).
17. We thank A. Mews for recording the luminescence spectra and A. Eychmüller for useful discussions.

30 August 1994; accepted 21 December 1994

Micrometer- and Nanometer-Sized Polymeric Light-Emitting Diodes

Magnus Granström,* Magnus Berggren, Olle Inganäs

A method for the fabrication of micrometer- and submicrometer-sized polymeric light-emitting diodes is presented. Such diodes have a variety of applications. Light sources of dimensions around 100 nanometers are required for subwavelength, near-field optical microscopy. Another possible application is patterning on the micrometer and nanometer scale. The diodes have been made in the form of a sandwich structure, with the conductive polymer poly(3,4-ethylene-dioxythiophene) polymerized in the pores of commercially available microfiltration membranes defining the hole-injecting contacts, poly[3-(4-octylphenyl)-2,2'-bithiophene] as the light-emitting layer, and a thin film of calcium-aluminum as the electron injector.

Since the first discoveries of electroluminescence in semiconducting conjugated polymers, interest has grown rapidly and many polymers have been used in light-emitting diodes (LEDs). The great interest is explained by the significant advantages that these systems have in processing, mechanical properties, and geometry possibilities as compared to conventional semiconductors (1–4). Another favorable aspect of the polymer LEDs is that today it is possible to cover the spectral range from blue to near-infrared, even within a single family of conductive polymers such as the polythiophenes (5). The recent demonstration of voltage-controlled electroluminescence colors from polymer blends in LEDs (5) as well as the possibility of obtaining polarized light from oriented polymers in LED devices (6) extend the possibilities of the polymer devices by comparison with inorganic devices. The mechanism for electroluminescence is also somewhat different from that found in conventional devices, because the emission takes place when charged po-

laron excitons recombine. When holes and electrons are injected into the polymer, they form positively and negatively charged polarons that can migrate under an applied field and radiatively recombine when they meet (7).

One of the advantages with polymer LEDs is the possibility to choose size and geometry freely. So far, this has mainly been exploited in making large (several square centimeters) LEDs. However, here we show that it is also possible to go in the other direction and make the light sources very small. Such LEDs could be used as light sources in scanning near-field optical microscopes (SNOMs), where the size of the emitting area is crucial (8, 9).

Two different conjugated polymers have been used in making these small LEDs. The first one, poly(3,4-ethylene-dioxythiophene) (10–13) (PEDOT) (1), was used as the hole-injecting contact; the other, poly[3-(4-octylphenyl)-2,2'-bithiophene] (14) (PTOPT) (2), was used as the electroluminescent layer (Fig. 1). To define the size of the light sources, we polymerized the doped and conducting polymer PEDOT electrochemically in the randomly distributed pores of commercially available microfiltration membranes (15, 16). The pore sizes in such mem-

Laboratory of Applied Physics, Department of Physics and Measurement Technology, Linköping University, S-581 83 Linköping, Sweden.

*To whom correspondence should be addressed.

branes span from 10 nm to 14 μm . Electrosynthesis of conjugated polymers inside these pores leads to high-conductivity materials, probably the result of increased ordering of the material (17, 18). It also leads to electrodes of the same size as the pores, if care is taken to stop the polymerization before the growing polymer extends beyond the narrow pore and starts to spread out on the upper surface of the membrane. This is therefore a convenient way to prepare small electrodes.

The electrode size is also expected to define the size of the light sources. Because the electron and hole mobilities are low in undoped conjugated polymers, the charges will not travel far from the injecting electrode. The upper limit of the exciton diffusion length in conjugated polymers has been estimated to be 5 nm (19), which also supports the idea that the light will be emitted only at or very close to the injecting contact.

Polycarbonate membranes (Poretics and Nuclepore) with pore diameters of 10 μm (thickness, 10 μm) and 100 nm (thickness, 6 μm) were attached to Au contacts on top of a glass substrate (16). We polymerized PEDOT from a water solution of 0.1 M monomer and 0.1 M sodium polystyrene sulfonate, using an electrochemical analyzer (Bioanalytical Systems BAS100A). A standard three-electrode setup was used with Ag-AgCl and Pt as reference and counter electrodes, respectively, and the polymerization potential was 1.3 V versus Ag-AgCl. The polymerization was interrupted when the conductive polymer fibers reached the upper surface of the membrane (16). This procedure produces a membrane surface with electrical contacts defined by the doped polymer fibers that have grown in the pores. All these fibers can then be electrically contacted through the Au layer between the glass substrate and the membrane.

The electroluminescent polymer PTOPT was spin-coated in its undoped form from a warm xylene solution (5 mg/ml, 50°C) on top of the membrane-contact structure. The thickness of this layer was estimated from optical spectra to be 350 to 450 \AA . To obtain

a suitable electron-injecting contact, we evaporated a thin layer of the low-work-function metal Ca (7) on the PTOPT surface. The Ca layer was then covered with a thin layer of Al to protect the Ca from the ambient atmosphere. The total thickness of the Al-Ca metal layer was 180 to 250 \AA . The resulting structure is shown in Fig. 2. The light is observed through the metal layer, resulting in a considerable decrease in light intensity.

We evaluated the diode structures using a computerized setup with an electrometer (Keithley 617), a picoammeter (Keithley 485), and a Si photodiode (Hamamatsu 1010BR). This setup makes it possible to measure the current-voltage (*I-V*) characteristics and light emission simultaneously. In addition to these measurements, an optical microscope (Olympus BHSP) equipped with a 35-mm camera was used to identify the individual light sources. In Fig. 3 a typical result from a 10- μm sample is shown. Comparing the current and light curves, it can be seen that one of the charge carriers starts to flow first, but no light is seen until both types are available and can recombine to give excitons (20). In Fig. 4 current and light curves for 100-nm diodes are shown. A similar behavior is found here, although with a lower light intensity because a smaller fraction of the surface is acting as a contact compared to the 10- μm samples (2.4% and 7.8%, respectively).

A photograph of the 100-nm LEDs is shown in Fig. 5. It is impossible to determine the exact size and shape of the light sources, because the optical microscope limits the resolution to 0.27 μm (magnification,

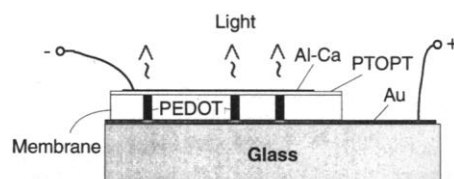


Fig. 2. Schematic of the proposed LED.

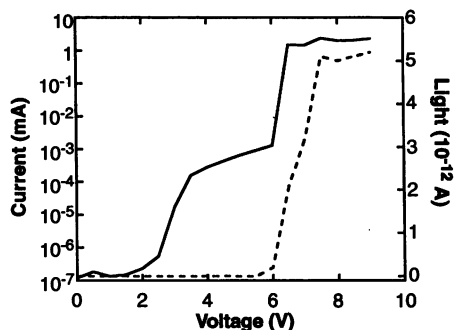


Fig. 3. Current (solid line) and light (dashed line) as functions of applied voltage for 10- μm diodes. The light is measured as the current from the photodiode.

$\times 1000$; numerical aperture, 1.25). However, it is still possible to detect the light and to establish an upper limit to the size of the LEDs of not more than 300 nm. This is then within the region of a subwavelength light source [the emission peak from "normal" PTOPT LEDs is at about 600 nm (14)].

From Figs. 3 and 4 the number of photons emitted per second from an individual diode can be estimated; this can be calculated from the current produced in the photodiode and knowledge of the emitting area. Two important factors need to be taken into account when such a calculation is performed. First, there is a statistical length distribution of the PEDOT fibers, because all pores in the membrane are not oriented perfectly perpendicular to the surface. Second, the diodes have different lifetimes, and a limiting factor for the lifetime of a diode is the heat expansion of the PEDOT contacts, which is attributable to the high current densities. An expanding PEDOT fiber can then break through the thin electroluminescent PTOPT layer and cause local "burnouts." The number of working diodes is therefore always smaller than the number of pores in the membrane.

From pictures taken in the microscope, the fraction of working diodes is found to be in the range of 20 to 25% for both types. Taking this into account, a calculation of the photon emission gives 10^4 photons per second for the 10- μm diodes and 10 photons

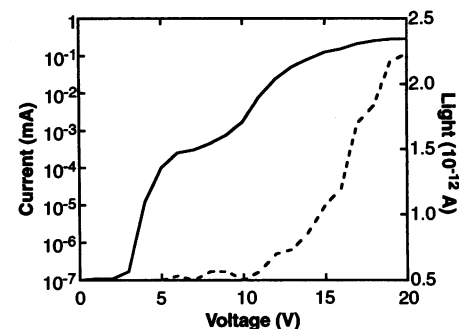


Fig. 4. Current (solid line) and light (dashed line) as a function of applied voltage for 100-nm diodes.



Fig. 5. Photo of nano-LEDs (100 nm) (magnification, $\times 1000$; exposure time, 15 min).

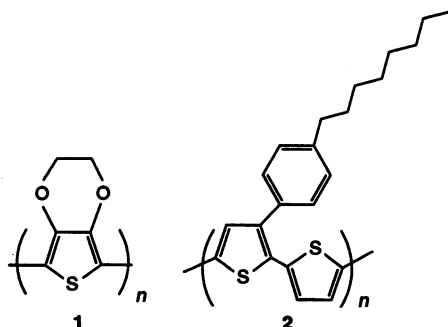


Fig. 1. Structures of compounds 1 and 2.

per second for the 100-nm diodes. The value for the 100-nm diodes is calculated directly from the optical image, where the diodes appear as 300-nm spots. If the diameter is assumed to be 100 nm, the number of photons per second increases by one order of magnitude to 10^2 . Looking at the quantum efficiencies established for large polymer LEDs in the family of polythiophenes, 0.1 to 1% external efficiencies, and current densities of 10 mA/cm^2 , we could expect 10^8 to 10^9 photons per second from the 10- μm LEDs and 10^4 to 10^5 photons per second from the 100-nm LEDs. Transmission losses in the metal electrode account for a part of this discrepancy and are measured by optical spectroscopy to be on the order of 60 to 80%. For our combination of materials, the quantum efficiency is most probably less than 0.1%, which, together with the transmission losses, brings the theoretical and experimental values into agreement with each other.

The numbers of emitted photons per second are calculated for the currents and voltages shown in the figures. It should be possible to increase these numbers by at least two orders of magnitude by increasing the current and using pulse techniques (21). As a comparison, it could be mentioned that one of the standard probes for SNOM, a tapered Al-coated optical fiber with a small aperture, suppresses the incoming light typically by a factor of 10^5 (8). Different techniques have been used with light intensities between 10^3 and 10^{11} photons per second for subwavelength light sources (22–24). We can then compare these results with projections of the best results for polymer nano-LEDs, where we may assume that we could increase efficiency to somewhere in the range of 1 to 10% and also that we might be able to operate the devices at current densities 10 times higher than those used presently. These developments would bring the photon emission up to the range of 10^7 to 10^8 photons per second, which puts the polymer nano-LEDs somewhere in the mid-range of the available techniques with respect to light intensity. Therefore, it should not be expected that polymer nano-LEDs would offer drastically better performance as subwavelength light sources than alternative devices. Rather, an advantage for the use of nano-LEDs may be in the ability to manufacture not one but thousands of light sources at the same time. This accomplishment might then be used to create efficient photopatterning processes that could be used to produce a large number of identical patterns simultaneously.

It may be possible in the future to improve a number of aspects of these structures—for instance, increasing the efficiency by using transport layers (20) or finding an appropriate transparent electron injector that could be used in this type of geometry.

The problem with heat expansion in the contacting polymer fibers could be reduced by using a much thinner insulating layer than the microfiltration membrane, in which small holes for polymerization could be made. The possibility of preparing thousands or millions of light sources at the same time, which is essential for some applications, may require methods such as ion-beam etching to control the distribution of light sources on the surface.

REFERENCES AND NOTES

1. J. H. Burroughes *et al.*, *Nature* **347**, 539 (1990).
2. D. Braun and A. J. Heeger, *Appl. Phys. Lett.* **58**, 1982 (1991).
3. G. Gustafsson *et al.*, *Nature* **357**, 477 (1992).
4. R. Friend, D. Bradley, A. Holmes, *Physics World* **1992**, 42 (1992).
5. M. Berggren *et al.*, *Nature* **372**, 444 (1994).
6. P. Dyreklev *et al.*, *Adv. Mater.*, in press.
7. I. D. Parker, *J. Appl. Phys.* **75**, 1656 (1994).
8. N. F. v. Hulst, M. H. P. Moers, B. Bölgel, *J. Microsc.* **171**, 95 (1993).
9. N. F. v. Hulst *et al.*, *Appl. Phys. Lett.* **62**, 461 (1993).
10. Q. Pei, G. Zuccarello, M. Ahlskog, O. Inganäs, *Polymer* **35**, 1347 (1994).

11. G. Heywang and F. Jonas, *Adv. Mater.* **4**, 116 (1992).
12. J. C. Gustafsson, B. Liedberg, O. Inganäs, *Solid State Ionics* **69**, 145 (1994).
13. M. Dietrich, J. Heinze, G. Heywang, F. Jonas, *J. Electrochem. Soc.* **369**, 87 (1994).
14. M. Berggren *et al.*, *J. Appl. Phys.*, in press.
15. Z. Cai and C. R. Martin, *J. Am. Chem. Soc.* **111**, 4138 (1989).
16. M. Granström and O. Inganäs, *Synth. Metals* **55–57**, 460 (1993).
17. Z. Cai, J. Lei, W. Liang, V. Menon, C. R. Martin, *Chem. Mater.* **3**, 960 (1991).
18. M. Granström and O. Inganäs, in preparation.
19. A. R. Brown *et al.*, *Chem. Phys. Lett.* **200**, 1 (1992).
20. A. R. Brown *et al.*, *Appl. Phys. Lett.* **61**, 2793 (1992).
21. D. Braun, D. Moses, C. Zhang, A. J. Heeger, *ibid.*, p. 3092.
22. N. Kuck, K. Lieberman, A. Lewis, A. Vecht, *ibid.*, p. 139.
23. A. Lewis and K. Lieberman, *Nature* **354**, 214 (1991).
24. E. Betzig, J. K. Trautman, T. D. Harris, J. S. Weiner, R. L. Kostelak, *Science* **251**, 1468 (1991).
25. We thank N. F. van Hulst and M. H. P. Moers for fruitful discussions. This work was supported by the Micronics program of the Swedish National Board for Industrial and Technical Development.

20 September 1994; accepted 19 December 1994

Influence of Lunar Phase on Daily Global Temperatures

Robert C. Balling Jr.* and Randall S. Cerveny

A newly available data set of daily satellite-derived, lower-tropospheric global temperature anomalies provides an opportunity to assess the influence of lunar phase on planetary temperature. These results reveal a statistically significant 0.02 K modulation between new moon and full moon, with the warmest daily global temperatures over a synodic month coincident with the occurrence of the full moon. Spectral analysis of the daily temperature record confirms the presence of a periodicity that matches the lunar synodic (29.53-day) cycle. The precision of the satellite-based daily temperature record allows verification that the moon exerts a discernible influence on the short-term, global temperature record.

Throughout history, many societies and individuals have believed that the moon exerts an influence on weather and climate. Indeed, scientists have been able to identify lunar-phase impacts on precipitation variations (1–4), thunderstorm frequency (5), ice nuclei concentrations (6), diurnal pressure changes (7), hurricanes (8), cloudiness as measured by sunshine recorders (9), and possibly global surface-temperature estimates (10). Adderley and Bowen (2, p. 749) claimed that “the appearance of a lunar component in daily temperature in certain parts of the world [is] comparatively well known” but is “extremely small and difficult to detect.” Until recently, the clear identification of a lunar influence on planetary temperature

was complicated by the lack of an accurate measure of global temperature on a daily basis.

A data set of significant reliability and sensitivity is now available that is potentially capable of being used to detect a lunar influence on global temperature. Spencer and Christy (11) have developed a lower-tropospheric (lowest 6 km) measure of global temperature based on microwave emissions of molecular oxygen. These microwave measurements are made by polar-orbiting satellites, thereby providing for coverage of the entire planet. The details of the measurement procedures are well documented, and this global data set is now widely used in climatic research (12–20). Although most scientists have used the monthly averaged, satellite-based temperature measurements, daily, globally averaged lower-tropospheric temperatures are now available (21,

Office of Climatology, Arizona State University, Tempe, AZ 85287, USA.

*To whom correspondence should be addressed.